

Polar metals as electrodes to suppress the critical-thickness limit in ferroelectric nanocapacitors

Danilo Puggioni,¹ Gianluca Giovannetti,² and James M. Rondinelli^{1,*}

¹*Department of Materials Science and Engineering, Northwestern University, IL 60208-3108, USA*

²*CNR-IOM-Democritos National Simulation Centre and International School for Advanced Studies (SISSA), Trieste, Italy*

(Dated: May 25, 2022)

Enhancing the performance of nanoscale ferroelectric (FE) field-effect transistors and FE capacitors for memory devices and logic relies on miniaturizing the metal electrode/ferroelectric area and reducing the thickness of the insulator. Although size reductions improve data retention, deliver lower voltage threshold switching, and increase areal density, they also degrade the functional electric polarization. There is a critical, nanometer length t_{FE}^* below which the polarization disappears owing to depolarizing field effects. Here we show how to overcome the critical thickness limit imposed on ferroelectricity by utilizing electrodes formed from a novel class of materials known as polar metals. Electronic structure calculations on symmetric polar-metal electrode/FE capacitor structures demonstrate that electric polarizations can persist to the sub-nanometer scale with $t_{\text{FE}}^* \rightarrow 0$ when a component of the polar axis in the electrode is perpendicular to the electrode/insulator interface. Our results reveal the importance of interfacial dipolar coherency in sustaining the polarization, which provides a platform for atomic scale structure-based design of functions that deteriorate in reduced dimensions.

I. INTRODUCTION

When ferroelectric oxides are utilized in metal/oxide heterostructures and nanocapacitors, scaling of the active FE is required to improve performance [1–3]. Nonetheless, deleterious nanoscale effects are amplified in these geometries [4–6] and act to eliminate the functional electric polarization [7–9]. The loss of ferroelectricity in nanoscale capacitors frequently occurs when the polarization is perpendicular to the film surface [4, 10–12], *i.e.*, the desired polarization direction for field-tunable devices [13]. Bound charges are only partially screened at the interface, resulting in a strong depolarizing field that suppresses the polarization. Indeed, numerous reports suggest a critical thickness, t_{FE}^* below which the electric polarization disappears. Experimental studies on PbTiO_3 find $t_{\text{FE}}^* \sim 20 \text{ \AA}$ at 300 K [14] whereas $t_{\text{FE}}^* \sim 4.0 \text{ nm}$, in $\text{Pb}(\text{Zr}_{0.2}\text{Ti}_{0.8})\text{O}_3$ films [8]. Furthermore, first-principles density functional theory (DFT) calculations predict $t_{\text{FE}}^* \sim 2.4 \text{ nm}$ in single-domain BaTiO_3 films between SrRuO_3 electrodes [4], which reduces to $t_{\text{FE}}^* \sim 1.0 \text{ nm}$ after accounting for ionic relaxation in the electrodes [5, 6]. With this limitation, ferroelectric based devices are unable to meet the continuous scaling changes demanded by higher density data storage technologies.

Although proposals to overcome the problem exist, a general solution remains elusive. Most approaches focus on tuning the stability of the FE state. Epitaxial strain engineering has been proposed; nonetheless, this strategy extends to a limited number of oxides, requires complex processing steps, and is limited by available commercial substrates. For example, although it is predicted that $t_{\text{FE}}^* \rightarrow 0$ in thin films of the incipient ferroelectric BaZrO_3 , a large epitaxial compressive strain of 4.25% is required [15], which would produce deleterious misfit dislocations. Integration with silicon is likely to also lead to uncontrolled interface states [16]. Furthermore, at this level of

strain t_{FE}^* is still finite for BaTiO_3 (Ref. 15).

Alternative solutions change the type of ferroelectric and the active inversion symmetry lifting mechanism. *Ab-initio* calculations find that $t_{\text{FE}}^* \rightarrow 0$ using so-called hyperferroelectrics [17], which have a persistent polarization different from proper FE oxides, or improper ferroelectrics [18, 19]. However, hyperferroelectric bulk materials (and thin films) remain to be synthesized [20]. Another route relies on creating an enhanced interfacial FE state by controlling the covalency of the metal-oxygen bond at the heterointerface [21–24].

Here we examine the critical thickness for ferroelectricity in nanocapacitors consisting of *polar-metal* electrodes and conventional ferroelectric oxides under short-circuit boundary conditions using DFT calculations. Recently, polar metals have garnered considerable interest [25, 26] because they exhibit simultaneously inversion-lifting displacements and metallicity. In these compounds, the polar displacements are weakly coupled to the states at the Fermi level, which makes possible the coexistence of a polar structure and metallicity [27]. Our main finding is that polar-metal electrodes suppress the critical thickness limit through interfacial polar displacements, which stabilize the ferroelectric (polarized) state; this geometric effect does not rely on interfacial bond chemistry or ‘perfect’ screening of the depolarizing field, but rather results from the intrinsic broken parity present in the electrode.

II. METHODS

We perform first-principles DFT calculations within the local-density approximation (LDA) and hybrid functional (HSE06, Ref. 28 and 29) as implemented in the Vienna *Ab initio* Simulation Package (VASP) [30] with the projector augmented wave (PAW) approach [31] to treat the core and valence electrons using the following electronic

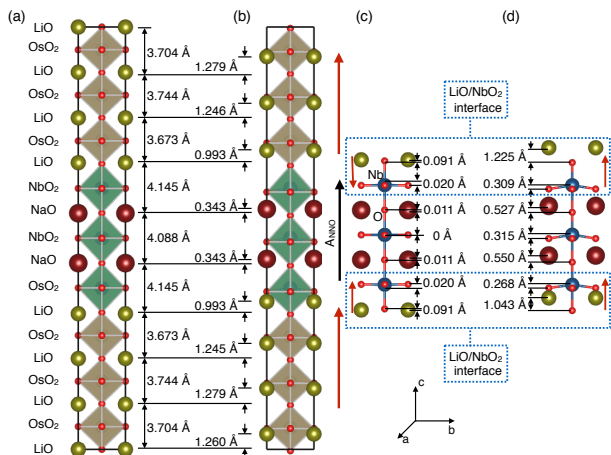


FIG. 1. Symmetric nanocapacitor consisting of polar-metal electrodes and a ferroelectric oxide. **a**, The centrosymmetric nanocapacitor with insulating NaNbO_3 ($m=2$) between LiOsO_3 electrodes ($n=6$). **b**, The equilibrium structure of the ferroelectric capacitor $[\text{LiO}-(\text{OsO}_2\text{-LiO})_6/\text{NbO}_2\text{-(NaO-NbO}_2)_2]$. The direction of the polar displacements in the electrodes and the ferroelectric film (A_{NNO}) are indicated with arrows. Magnification of the **c**, paraelectric aristotype and **d**, the ground state structure. The FE behavior at the interface is due to the Li, Nb, and O displacements. The direction of the polar displacements at the interfaces for the paraelectric and the ground state structure is indicated with red arrows.

configurations: $1s^2 2s^2$ (Li), $5p^6 6s^2 5d^6$ (Os), $2s^2 2p^4$ (O), $5s^2 5p^6 6s^2$ (Ba), $3d^2 4s^2$ (Ti), $4s^2 4p^6 5s^2$ (Sr), $4d^7 5s^1$ (Ru), $2p^6 3s^1$ (Na), $4p^6 4d^4 5s^1$ (Nb). The Brillouin zone integrations are performed with a $13 \times 13 \times 1$ Monkhorst-Pack k -point mesh [32] and a 600 eV plane wave cutoff for the $\text{LiOsO}_3/\text{NaNbO}_3/\text{LiOsO}_3$ and $\text{SrRuO}_3/\text{BaTiO}_3/\text{SrRuO}_3$ capacitor structures. We relax the atomic positions (force tolerance less than $0.1 \text{ meV } \text{\AA}^{-1}$) using Gaussian smearing (20 meV width).

Below 150 K NaNbO_3 and LiOsO_3 are isostructural with rhombohedral space group $R3c$ and pseudocubic lattice parameters of 3.907 \AA (Ref. 33) and 3.650 \AA (Ref. 25), respectively. Owing to the large lattice mismatch between the two compounds, we simulate a symmetric ferroelectric capacitor structure with an LiO/NbO_2 interfacial termination, shown in Fig. 1a, under an epitaxial constraint that would be imposed by a $(\text{La}_{0.3}\text{Sr}_{0.7})(\text{Al}_{0.65}\text{Ta}_{0.35})\text{O}_3$ substrate [34] and we relax the out-of-plane lattice parameter. This results in a compressive strain of $\sim 1\%$ for NaNbO_3 and a tensile strain of $\sim 6\%$ for LiOsO_3 . Note that at the bulk level, we find that a tensile strain $\gtrsim 6\%$ suppresses the polar instability along the $[001]$ -pseudocubic direction of LiOsO_3 . Moreover, we selected NaNbO_3 for the capacitor structures because to eliminate any charge transfer due to ‘polar catastrophe/charge mismatch’ physics as the interface: $[\text{LiO}]^{1-}$, $[\text{NaO}]^{1-}$, $[\text{NbO}_2]^{1+}$, and $[\text{OsO}_2]^{1+}$.

For the two ferroelectric capacitors, we adopt the layered-oxide notation used in Ref. 4, that is

- $[\text{LiO}-(\text{OsO}_2\text{-LiO})_n/\text{NbO}_2\text{-(NaO-NbO}_2)_m]$ and
- $[\text{SrO}-(\text{RuO}_2\text{-SrO})_n/\text{TiO}_2\text{-(BaO-TiO}_2)_m]$

to clearly demarcate the interface composition in the $\text{LiOsO}_3/\text{NaNbO}_3/\text{LiOsO}_3$ and $\text{SrRuO}_3/\text{BaTiO}_3/\text{SrRuO}_3$ capacitors, respectively. We use a LiO/NbO_2 electrode/ferroelectric interface for the $\text{LiOsO}_3/\text{NaNbO}_3/\text{LiOsO}_3$ capacitor and a SrO/TiO_2 interface termination for the $\text{SrRuO}_3/\text{BaTiO}_3/\text{SrRuO}_3$ capacitor. For both ferroelectric capacitors, we constrained the number of 5-atom perovskite units of the electrode at $n = 6$ to ensure a thickness large enough to avoid interaction between the two interfaces, and m ranged from 1 to 3. The periodic boundary conditions naturally impose the required short-circuit condition between the electrodes. Note that for $\text{SrRuO}_3/\text{BaTiO}_3/\text{SrRuO}_3$ capacitors, our geometry differs only slightly from that used by Junquera and Ghosez [4], whereby the thickness of our electrode is greater.

The group theoretical analysis was aided by the ISODISTORT software [35]. It is used to evaluate the geometric-induced inversion symmetry-breaking displacements of the $P4mm$ structure with respect the $P4/mmm$ phase, reducing the polar structure into a set of symmetry-adapted modes associated with different irreducible representations of the $P4/mmm$ phase. The ‘robust’ algorithm was used to match an atom in the undistorted structure to every atom in the distorted structure separated by a threshold distance less than 3 \AA .

III. RESULTS AND DISCUSSION

The first ferroelectric nanocapacitor we focus on consists of ferroelectric NaNbO_3 of varying thickness m confined between electrodes of the experimentally known polar metal LiOsO_3 (see Fig. 1, $m = 2$) [25, 36]. We adopt the layered-oxide notation used in Ref. 4, that is $[\text{LiO}-(\text{OsO}_2\text{-LiO})_n/\text{NbO}_2\text{-(NaO-NbO}_2)_m]$ to clearly demarcate the interface composition (see Methods). We create two symmetric nanocapacitors with a polar and paraelectric configuration for both LiOsO_3 and NaNbO_3 , respectively. We then relax the out-of-plane lattice parameter and the atomic positions of the nanocapacitors for $m=1, 2$, and 3. The lowest energy heterostructures are polar with space group $P4mm$ and exhibit large Li ions displacements along the $[001]$ -pseudocubic direction (Fig. 1b). No zone-center dynamical instabilities are found in these heterostructures. Note that structures with an initial paraelectric configuration relax into a centrosymmetric structure (space group $P4/mmm$) with Li atoms displaying large antipolar displacements in LiOsO_3 (Supplementary Fig. 1) that decrease towards the interface (Fig. 1c).

We use representation theory analysis to examine the inversion lifting distortions (see Methods), and find that the distortion vector corresponds to the irreps Γ_1^+ and Γ_3^- . The irrep Γ_1^+ reduces the antipolar displacements

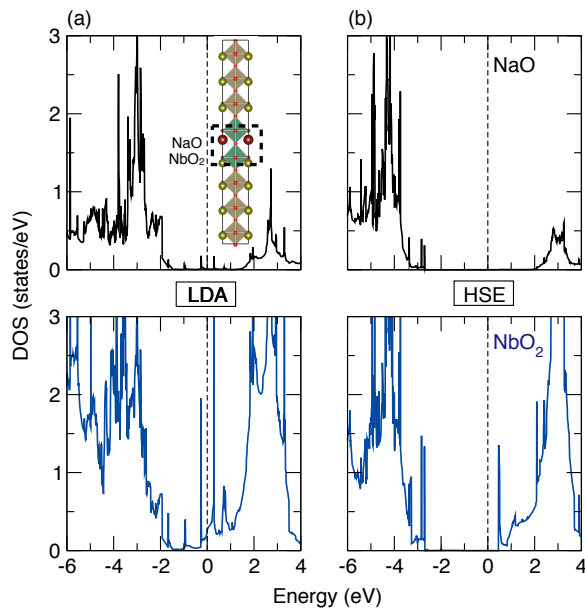


FIG. 2. Projected densities-of-states (DOS) for the NaNbO_3 layer in the $\text{LiOsO}_3/\text{NaNbO}_3/\text{LiOsO}_3$ ($m=1$) nanocapacitor within **a**, LDA and **b**, HSE06. The inset shows the $\text{LiOsO}_3/\text{NaNbO}_3/\text{LiOsO}_3$ ($m=1$) nanocapacitor.

in LiOsO_3 resulting in the centrosymmetric $P4/mmm$ structure depicted in Fig. 1a. Differently, the irrep Γ_3^- is a polar mode which involves mainly Li ion displacements—the maximum amplitudes being ~ 1.3 Å in LiOsO_3 with decreasing amplitude towards the LiO/NbO_2 interface (Fig. 1b). It also consists of polar displacements of all ions in the dielectric NaNbO_3 layers with the Nb ions off-centering the most (Fig. 1d)

For all thicknesses, the NaNbO_3 thin film maintains a ferroelectric ground state characterized by both Nb and Na displacements (Fig. 1b). A linear polarization-displacement model using the Born effective charge from Ref. 37 results in a 0.86 C m^{-2} polarization for NaNbO_3 in $m=2$. An analysis of the differential ionic relaxations in the heterostructure reveals polar displacements at the LiO/NbO_2 interfaces—an interfacial ferroelectricity—which are a consequence of the polar metal used as an electrode. This produces an enhanced polarization in the ferroelectric compared to that calculated using the aforementioned procedure in the experimental $R3c$ structure (0.59 C m^{-2}) [38]. In particular, although the two interfaces of the paraelectric structures exhibit *antiparallel* polar displacements (Fig. 1c and Supplementary Fig. 1), the interfaces of the polar ground state structures have *parallel* polar displacements as show in Fig. 1d.

Fig. 2 shows the electronic properties for the NaNbO_3 layer in the $\text{LiOsO}_3/\text{NaNbO}_3/\text{LiOsO}_3$ ($m=1$) nanocapacitor. The LDA functional predicts that the NaNbO_3 film is metallic, rendering the ferroelectric capacitor unusable (Fig. 2a). This behavior is artificial and due to the tendency of the LDA functional to underestimate the band gap in insulating compound [39, 40]. We solve

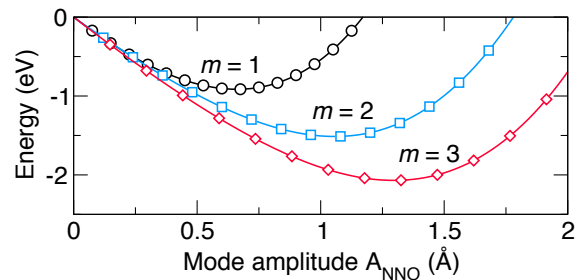


FIG. 3. Energetic gain with increasing polar mode amplitude \mathcal{A}_{NNO} in the NaNbO_3 film for different thicknesses: $m=1$ (circles), $m=2$ (squares) and $m=3$ (diamonds). A finite value of \mathcal{A}_{NNO} leads to an energetic gain for all m , indicating the disappearance of the critical thickness. Note that the energy of the polar ground state structure with $\mathcal{A}_{\text{NNO}}=0$ Å is taken as reference for each value of m . As expected the energy gain increases as the thickness of the ferroelectric film increases owing to the reduced effects from the depolarizing field, which dominates thinner films.

this pathological problem for DFT by using a more sophisticated functional which includes a fraction of exact exchange (HSE06). Fig. 2b shows that the hybrid functional fully opens the gap between the O $2p$ and Nb $4d$ states. Moreover, we find that the HSE06-relaxed structures exhibit displacements similar to those obtained from the LDA functional; importantly, polar displacements at the LiO/NbO_2 interfaces. This result supports the conclusion that the interfacial ferroelectricity is induced by the polar crystal structure of the metallic electrode and not due to spurious shorting of the capacitor. In the remainder of this paper, we report results obtained using LDA owing to the similar crystal structure obtained with HSE06 functional.

Fig. 3 shows the evolution of the total energy of each capacitor with mode amplitude \mathcal{A}_{NNO} , which describes the atomic displacements involved in the soft mode of the NaNbO_3 film. As expected the largest energy gain occurs when the thickness of the ferroelectric film increases. Note that the shape of the energy surface does not exhibit the characteristic double well behavior, because in our calculations we fix the polar displacements in the metallic electrodes and only change the amplitude of the polar displacements in NaNbO_3 . Independent of the NaNbO_3 film thickness, the energy is minimized for the ferroelectric ground state ($\mathcal{A}_{\text{NNO}} \neq 0$), indicating that an ideal ferroelectric capacitor can be reduced to an ultrathin (single unit cell) size, i.e., $t_{\text{FE}}^* \rightarrow 0$.

The disappearance of the critical-thickness limit to ferroelectricity is the result of the parallel polar displacements present at the electrode/dielectric interfaces (Fig. 1b). As proposed in Ref. 22, the ferroelectric state in ultrathin-film devices depends crucially on the nature of the chemical bonds at the metal/oxide interface. Here, this interfacial bonding occurs and is an immediate consequence of the structure of the polar-metal electrodes. The enhanced and parallel interfacial polar displacements

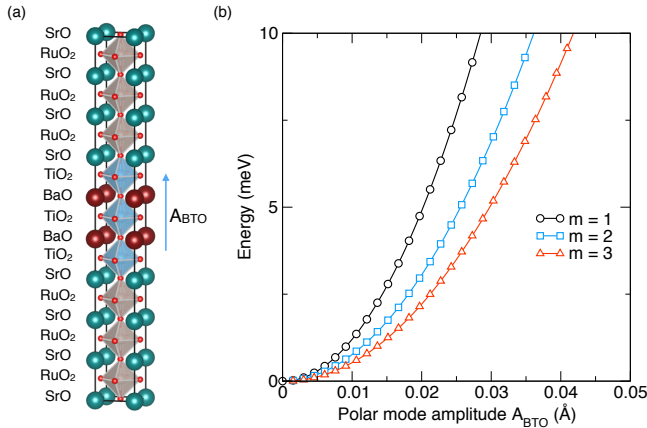


FIG. 4. Typical behavior of a nanoscale ferroelectric capacitor below the critical thickness. **a**, Nanocapacitor consisting of a BaTiO₃ film ($m=2$) between centrosymmetric SrRuO₃ ($n=6$) electrodes. The arrow indicates the direction of the polar displacements in BaTiO₃. **b**, Energy as a function of the polar mode amplitude A_{BTO} in BaTiO₃. The energy increases for all thicknesses m analyzed.

“imprint” and lead to an overall enhancement of the ferroelectric instability of the film, which we assess further below. We stress that differently from Ref. 22, the interfacial dipole distortions are due to a geometrical mechanism driven by the polar structure of the metallic electrode and not due to the stiffness of the electrode–oxide bonds.

We next examine a SrRuO₃/BaTiO₃/SrRuO₃ capacitor (Fig. 4a), which as before may be written as [SrO-(RuO₂-SrO) _{n} /TiO₂-(BaO-TiO₂) _{m}] to reveal the layered monoxide planes in the structures. We focus on the SrO/TiO₂ interface geometry to demonstrate the generality of this solution to the critical thickness problem. We constrain the in-plane lattice parameters to that of SrTiO₃ (3.905 Å) and we relax the out-of-plane lattice parameter and the atomic positions (see Methods), examining capacitors with $m=1, 2$, and 3 that are well below the reported $m=7$ critical thickness [4]. With nonpolar SrRuO₃ electrodes the paraelectric configuration is energetically more stable than the ferroelectric configuration for all BaTiO₃ film thicknesses studied. This is confirmed by the increase in total energy as a function of the polar mode amplitude A_{BTO} (Fig. 4b). Indeed, the use of a centrosymmetric metal for the thinnest ferroelectric film results in an antisymmetric poling effect of the two interfaces, which forbids the possibility of a ferroelectric displacement [5].

Now we perform a computational experiment whereby we transmute centric SrRuO₃ into a hypothetical polar metal by following the design rules for noncentrosymmetric metals introduced in Ref. 27. We do this by imposing a polar distortion in SrRuO₃, which involves only the Sr atoms, as the orbital character at the Fermi level has a negligible contribution from these atoms, with parallel polar displacements at the SrO/TiO₂ interfaces as suggested by our LiOsO₃/NaNbO₃/LiOsO₃ capacitor results. We

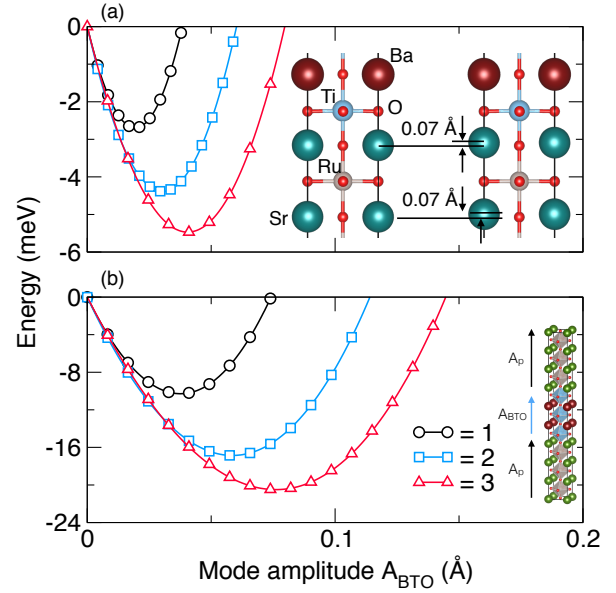


FIG. 5. Energetic landscape of a BaTiO₃ nanocapacitor with “polar” SrRuO₃ electrodes. Energetic gain for different dielectric thicknesses: $m=1$ (circles), $m=2$ (squares) and $m=3$ (diamonds). The Sr displacements given with respect to the centrosymmetric ground state are fixed to **a**, 0.07 Å (see inset) and **b**, 0.14 Å. The energy of the polar structure with $A_{\text{BTO}}=0$ Å is taken as reference for each m .

point out that bulk SrRuO₃ does not exhibit polar distortions and here we make it artificially polar to isolate the interfacial geometric effect independent of chemistry with respect to the model with centrosymmetric electrodes.

In Fig. 5a we show the energy evolution of this hypothetical capacitor as a function of the mode amplitude A_{BTO} , with parallel polar Sr displacements imposed uniformly at 0.07 Å with respect to the centrosymmetric structure (see inset). In contrast to Fig. 4a, the ferroelectric state of BaTiO₃ is more stable than the paraelectric geometry for all thicknesses $m=1, 2$, and 3 as indicated by the energy gain for $A_{\text{BTO}} \neq 0$. These results indicate that $t_{\text{FE}}^* \rightarrow 0$ in the BaTiO₃ film between the polar-metal SrRuO₃.

The energy gain is strongly influenced by the polar displacements of the Sr atoms. In particular, by doubling the amplitude of the polar displacements of the Sr atoms, from 0.07 Å to 0.14 Å for the case $m=1$, we find that the energy gain increases from ~ 3 meV to ~ 10 meV (Fig. 5b). Comparing Fig. 5a and Fig. 5b, we find a shift in the critical mode amplitude to larger values, which suggests that the device containing a polar-metal electrode with larger Sr displacements displays a larger ferroelectric polarization. Indeed, when we consider the other limit by fully removing the polar displacements at the SrO/TiO₂ interface (setting them to 0 Å), the energy landscape presented in Fig. 4b is restored. Note that for the disappearance of the critical thickness, it is necessary that the polar direction (or a component of it) in the electrodes, and therefore that of the interfacial dipole, coincides with the direction of

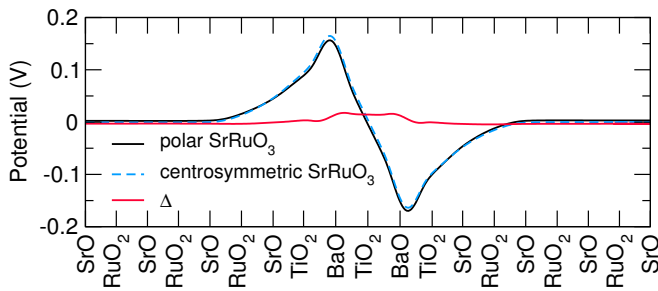


FIG. 6. The planar and macroscopically averaged electrostatic potential of the BaTiO₃ ferrocapacitor ($m=2$) along [001] between polar (solid line) and centrosymmetric (broken line) SrRuO₃ electrodes. The difference, Δ , is also shown. The amplitude of the polar distortion in the BaTiO₃ film is fixed to ~ 0.6 Å, which corresponds to the minimum in Fig. 5b. The configuration with paraelectric BaTiO₃ is used as reference.

polarization of the ferroelectric film (Fig. 5b, inset).

One could argue that the findings here are a result of the polar metals better screening the ferroelectrics polarization; however, this is not the case. Indeed the electrostatic for the BaTiO₃ nanocapacitor with “polar” and nonpolar SrRuO₃ electrodes are almost the same (Fig. 6). Moreover, polar metals typically have longer screening lengths than conventional metals [41]. This result further confirms the role of interfacial geometric effects induced by the polar structure of the metallic electrode in controlling the critical thickness.

Lastly, we discuss how the proposed device can be switched. Polar metals are not ferroelectrics. Indeed, the application of an electric field cannot switch the polar distortion in the metal because the free electrons will screen the electric field. However, it has been show that the polar distortion in the metal can be switched by applying an electric field to a superlattice composed of an insulating ferroelectric material and a polar metal by

coupling to the ferroelectric polarization [42]. Similarly, when an electric field is applied to the aforementioned nanocapacitors, the polar distortion in the ferroelectric thin film should align along the direction of the electric field; then because of the interfacial coupling between the polar metallic electrode and the ferroelectric film [42], the polar displacements in the polar metal and the interfacial polar displacements should follow. Note that the geometric configuration required to sustain ferroelectricity, *i.e.*, $t_{\text{FE}}^* \rightarrow 0$, is preserved in the switching mechanism. Alternative approaches have also been applied to degenerately doped ferroelectrics.[43]

IV. CONCLUSION

In summary, we proposed a ferroelectric capacitor where the conventional metallic electrodes are replaced by *non-centrosymmetric* metallic electrodes. We showed that the polar displacements in the noncentrosymmetric metallic electrodes induce interfacial ferroelectricity, which supports a polar instability in the ferroelectric film regardless of the dielectric thickness. Although we utilized LiOsO₃ herein for simplicity, we point out that our result is completely general and the same conclusions may be achieved using other noncentrosymmetric metals as electrodes with our described geometric constraints (see Ref. 44 for a list of materials). These polar-metal based nanoscale capacitors maintain the functionality of the ferroelectric film independent of the degree of miniaturization and could lead to device architectures with improved scalability.

ACKNOWLEDGMENTS

D.P. and J.M.R. acknowledge the Army Research Office under Grant No. W911NF-15-1-0017 for financial support and the DOD-HPCMP for computational resources.

* jronidelli@northwestern.edu

- [1] H. Ishiwara, M. Okuyama, and Y. Arimoto, *Ferroelectric Random Access Memories: Fundamentals and Applications* (Springer, Berlin, Germany, 2004).
- [2] G. Muller, N. Nagel, C. U. Pinnow, and T. Rohr, “Emerging non-volatile memory technologies,” in *Solid-State Circuits Conference, 2003. ESSCIRC '03. Proceedings of the 29th European* (2003) pp. 37–44.
- [3] J. F. Scott, “Future issues in ferroelectric miniaturization,” *Ferroelectrics* **206**, 365–379 (1998), <http://dx.doi.org/10.1080/001150199808009170>.
- [4] Javier Junquera and Philippe Ghosez, “Critical thickness for ferroelectricity in perovskite ultrathin films,” *Nature* **422**, 506–509 (2003).
- [5] G. Gerra, A. K. Tagantsev, N. Setter, and K. Parlinski, “Ionic polarizability of conductive metal oxides and critical thickness for ferroelectricity in batio₃,” *Phys. Rev. Lett.* **96**, 107603 (2006).
- [6] G. Gerra, A. K. Tagantsev, N. Setter, and K. Parlinski, “Erratum: Ionic polarizability of conductive metal oxides and critical thickness for ferroelectricity in batio₃ [phys. rev. lett. **96**, 107603 (2006)],” *Phys. Rev. Lett.*, 169904 (2007).
- [7] Kenji Ishikawa, Takashi Nomura, Nagaya Okada, and Kazumasa Takada, “Size effect on the phase transition in p b t i o 3 fine particles,” *Japanese Journal of Applied Physics* **35**, 5196 (1996).
- [8] T. Tybell, C. H. Ahn, and J.-M. Triscone, “Ferroelectricity in thin perovskite films,” *Applied Physics Letters* **75**, 856–858 (1999).
- [9] B. Jiang, J. L. Peng, L. A. Bursill, and W. L. Zhong, “Size effects on ferroelectricity of ultrafine particles of pbti₃,” *Journal of Applied Physics* **87**, 3462–3467 (2000).
- [10] Ph. Ghosez and K. M. Rabe, “Microscopic model of ferroelectricity in stress-free pbti₃ ultrathin films,” *Applied Physics Letters* **76**, 2767–2769 (2000).

- [11] B. Meyer and David Vanderbilt, “*Ab initio* study of BaTiO_3 and PbTiO_3 surfaces in external electric fields,” *Phys. Rev. B* **63**, 205426 (2001).
- [12] Igor Kornev, Huaxiang Fu, and L. Bellaiche, “Ultra-thin films of ferroelectric solid solutions under a residual depolarizing field,” *Phys. Rev. Lett.* **93**, 196104 (2004).
- [13] R. Ramesh and D. G. Schlom, “MATERIALS SCIENCE: Orienting Ferroelectric Films,” *Science* **296**, 1975–1976 (2002).
- [14] L. Despont, C. Koitzsch, F. Clerc, M. G. Garnier, P. Aebi, C. Lichtensteiger, J.-M. Triscone, F. J. Garcia de Abajo, E. Bousquet, and Ph. Ghosez, “Direct evidence for ferroelectric polar distortion in ultrathin lead titanate perovskite films,” *Phys. Rev. B* **73**, 094110 (2006).
- [15] Yajun Zhang, Gui-Ping Li, Takahiro Shimada, Jie Wang, and Takayuki Kitamura, “Disappearance of ferroelectric critical thickness in epitaxial ultrathin BaZrO_3 films,” *Phys. Rev. B* **90**, 184107 (2014).
- [16] John Hirth, *Dislocations in Solids* (Elsevier, 2008).
- [17] Kevin F. Garrity, Karin M. Rabe, and David Vanderbilt, “Hyperferroelectrics: Proper ferroelectrics with persistent polarization,” *Phys. Rev. Lett.* **112**, 127601 (2014).
- [18] Massimiliano Stengel, Craig J. Fennie, and Philippe Ghosez, “Electrical properties of improper ferroelectrics from first principles,” *Phys. Rev. B* **86**, 094112 (2012).
- [19] Na Sai, Craig J. Fennie, and Alexander A. Demkov, “Absence of critical thickness in an ultrathin improper ferroelectric film,” *Phys. Rev. Lett.* **102**, 107601 (2009).
- [20] Joseph W. Bennett, Kevin F. Garrity, Karin M. Rabe, and David Vanderbilt, “Hexagonal *abc* semiconductors as ferroelectrics,” *Phys. Rev. Lett.* **109**, 167602 (2012).
- [21] M. Stengel and N. A. Spaldin, “Origin of the dielectric dead layer in nanoscale capacitors,” *Nature* **443**, 679–682 (2006).
- [22] Massimiliano Stengel, David Vanderbilt, and Nicola A. Spaldin, “Enhancement of ferroelectricity at metal-oxide interfaces,” *Nature Materials* **8**, 392–397 (2009).
- [23] Meng-Qiu Cai, Yue Zheng, Pui-Wai Ma, and C. H. Woo, “Vanishing critical thickness in asymmetric ferroelectric tunnel junctions: First principle simulations,” *Journal of Applied Physics* **109**, 024103 (2011).
- [24] Hiroyuki Yamada, Atsushi Tsurumaki-Fukuchi, Masaki Kobayashi, Takuro Nagai, Yoshikiyo Toyosaki, Hiroshi Kumigashira, and Akihito Sawa, “Strong Surface-Termination Effect on Electroresistance in Ferroelectric Tunnel Junctions,” *Advanced Functional Materials* **25**, 2708–2714 (2015).
- [25] Youguo Shi, Yanfeng Guo, Xia Wang, Andrew J. Princep, Dmitry Khalyavin, Pascal Manuel, Yuichi Michiue, Akira Sato, Kenji Tsuda, Shan Yu, Masao Arai, Yuichi Shirako, Masaki Akaogi, Nanlin Wang, Kazunari Yamaura, and Andrew T. Boothroyd, “A ferroelectric-like structural transition in a metal,” *Nature Materials* **12**, 1024 (2013).
- [26] T. H. Kim, D. Puggioni, Y. Yuan, H. Zhou L. Xie, N. Campbell, P. J. Ryan, Y. Choi, J.-W. Kim, J. R. Patzner, S. Ryu, J. P. Podkaminer, J. Irwin, Y. Ma, C. J. Fennie, M. S. Rzechowski, V. Gopalan X. Q. Pan, J. M. Rondinelli, and C. B. Eom, “Polar metals by geometric design,” *Nature* **533**, 68–72 (2016).
- [27] Danilo Puggioni and James M. Rondinelli, “Designing a robustly metallic noncentrosymmetric ruthenate oxide with large thermopower anisotropy,” *Nat. Commun.* **5**, 3432 (2013).
- [28] Jochen Heyd, Gustavo E. Scuseria, and Matthias Ernzerhof, “Hybrid functionals based on a screened coulomb potential,” *J. Chem. Phys.* **118**, 8207–8215 (2003).
- [29] Jochen Heyd, Gustavo E. Scuseria, and Matthias Ernzerhof, “Erratum: hybrid functionals based on a screened coulomb potential [j. chem. phys.118, 8207 (2003)],” *J. Chem. Phys.* **124**, 219906 (2006).
- [30] G. Kresse and J. Furthmüller, “Efficiency of ab-initio total energy calculations for metals and semiconductors using a plane-wave basis set,” *Computational Materials Science* **6**, 15 – 50 (1996).
- [31] Peter E. Blöchl, O. Jepsen, and O. K. Andersen, “Improved tetrahedron method for brillouin-zone integrations,” *Physical Review B* **49**, 16223–16233 (1994).
- [32] Hendrik J. Monkhorst and James D. Pack, “Special points for Brillouin-zone integrations,” *Physical Review B* **13**, 5188–5192 (1976).
- [33] Seidel P. and Hoffmann W, “Verfeinerung der kristallstruktur von NaNbO_3 ,” *Zeitschrift für Kristallographie* **143**, 444–459 (1976).
- [34] J. Liu, M. Kargarian, M. Kareev, B. Gray, Phil J. Ryan, A. Cruz, N. Tahir, Yi-De Chuang, J. Guo, James M. Rondinelli, John W. Freeland, Gregory A. Fiete, and J. Chakhalian, “Heterointerface engineered electronic and magnetic phases of NdNiO_3 thin films,” *Nat. Commun.* **4**, 3714 (2013).
- [35] Branton J. Campbell, Harold T. Stokes, David E. Tanner, and Dorian M. Hatch, “*ISODISPLACE*: a web-based tool for exploring structural distortions,” *Journal of Applied Crystallography* **39**, 607–614 (2006).
- [36] Gianluca Giovannetti and Massimo Capone, “Dual nature of the ferroelectric and metallic state in LiOsO_3 ,” *Phys. Rev. B* **90**, 195113 (2014).
- [37] W. Zhong, R. D. King-Smith, and David Vanderbilt, “Giant lo-to splittings in perovskite ferroelectrics,” *Phys. Rev. Lett.* **72**, 3618–3621 (1994).
- [38] S. K. Mishra, N. Choudhury, S. L. Chaplot, P. S. R. Krishna, and R. Mittal, “Competing antiferroelectric and ferroelectric interactions in NaNbO_3 : Neutron diffraction and theoretical studies,” *Phys. Rev. B* **76**, 024110 (2007).
- [39] John P. Perdew, “Density functional theory and the band gap problem,” *International Journal of Quantum Chemistry* **28**, 497–523 (1985).
- [40] Massimiliano Stengel, Pablo Aguado-Puente, Nicola A. Spaldin, and Javier Junquera, “Band alignment at metal/ferroelectric interfaces: Insights and artifacts from first principles,” *Phys. Rev. B* **83**, 235112 (2011).
- [41] Gianluca Giovannetti, Danilo Puggioni, James M. Rondinelli, and Massimo Capone, “Interplay between electron correlations and polar displacements in metallic $\text{SrEuMo}_2\text{O}_6$,” *Phys. Rev. B* **93**, 115147 (2016).
- [42] H. J. Xiang, “Origin of polar distortion in LiNbO_3 -type ‘ferroelectric’ metals: Role of A-site instability and short-range interactions,” *Phys. Rev. B* **90**, 094108 (2014).
- [43] Pavan Nukala, Mingliang Ren, Rahul Agarwal, Jacob Berger, Gerui Liu, A. T. Charlie Johnson, and Ritesh Agarwal, “Inverting polar domains via electrical pulsing in metallic germanium telluride,” *Nat. Commun.* **8**, 15033 (2017).
- [44] Nicole A. Benedek and Turan Birol, “‘ferroelectric’ metals reexamined: fundamental mechanisms and design considerations for new materials,” *J. Mater. Chem. C* **4**, 4000–4015 (2016).